Endocardial HDAC3 is required for myocardial trabeculation

Jihyun Jang[1,2], Mette Bentsen[3], Ye Jun Kim[4], Erick Kim[4], Vidu Garg[1,2], Chen-Leng Cai[5], Mario Looso[3], Deqiang Li[1, 2]

[1]Center for Cardiovascular Research, Abigail Wexner Research Institute, Nationwide Children's Hospital, Columbus, OH 43215, USA

[2]Department of Pediatrics, The Ohio State University College of Medicine, Columbus, OH 43215, USA

[3]Bioinformatics Core Unit (BCU), Max Planck Institute for Heart and Lung Research, 61231, Bad Nauheim, Germany

[4]Department of Surgery, University of Maryland School of Medicine, Baltimore, MD 21201, USA

[5]Department of Pediatrics, Herman Wells Center for Pediatric Research, Indiana University School of Medicine, Indianapolis, IN 46201, USA

Address correspondence to:

Deqiang Li, MD&PhD

575 Children's Drive, Room WB4329,

Columbus, OH 43215, USA

Phone: 614-355-5826

Email: Deqiang.Li@nationwidechildrens.org

Abstract

Failure of proper ventricular trabeculation is often associated with congenital heart disease (CHD). Support from endocardial cells, including the secretion of extracellular matrix (ECM) and growth factors is critical for trabeculation. However, it is poorly understood how the secretion of ECM and growth factors is initiated and regulated by endocardial cells.

We found that genetic knockout (KO) of histone deacetylase 3 (*Hdac3*) in the endocardium in mice resulted in early embryo lethality and ventricular hypotrabeculation. Single cell RNA sequencing identified significant downregulation of ECM components in *Hdac3* KO endocardial cells. Secretome from cultured *Hdac3* KO mouse cardiac endothelial cells lacked transforming growth factor ß3 (TGFß3) and showed significantly reduced capacity in stimulating cultured cardiomyocyte proliferation, which was remarkably rescued by TGFß3 supplementation. Mechanistically, we identified that HDAC3 induced *Tgfß3* expression through repressing microRNA(miR)-129-5p.

Our findings provide novel insights into the pathogenesis of CHD and conceptual strategies to promote myocardial regeneration.

Introduction

Congenital heart disease (CHD) is the most common congenital disorder, and the leading cause of mortality from birth defects[1]. Defective myocardial growth is either the primary manifestation or associated with many forms of CHD[2, 3]. In the early primitive heart (mouse embryonic day 8-10), inner cardiac endothelial cells (CECs), also called endocardial cells, and outer cardiomyocytes (CMs), which are separated by extracellular matrix (ECM), co-contribute to early myocardial trabeculation (i.e., formation of myocardial meshwork extending to cardiac chamber)[4-6]. CECs juxtapose myocardial trabeculae and lead myocardial trabeculation by secretion of growth factors such as Neuregulin 1 (NRG1) and transforming growth factor ß (TGFß)[2, 3, 5]. Meanwhile, CECs support trabeculation by secreting ECM (e.g., various collagens, versican) that facilitate the travelling of CEC secreted growth factors to trabecular myocardium and support trabecular CM proliferation[4, 7]. Surprisingly, disruption of ECM components alone (e.g., hyaluronan synthase-2, versican) prevents the proper formation of trabeculae in mice[8, 9]. Although CECs play such important roles during ventricular trabeculation, it remains poorly understood how these ECM proteins and growth factors are regulated in the developing CECs.

TGFß signaling pathway is involved in many fundamental cellular processes in both adults and developing embryos including cell proliferation, differentiation, migration, and apoptosis[10, 11]. The TGFß superfamily includes many different ligands (e.g., Bone morphogenetic proteins, Growth and differentiation factors, Activin, Nodal, TGFß). These ligands bind to their specific type II receptors, which triggers phosphorylation of type I receptor, eventually leads to phosphor-Smad2/3 localized to the nucleus and drives a

64 variety of downstream target gene expression, which is the canonical TGFß signaling
65 pathway[12]. In addition, the binding of ligands to receptors can also directly activate
66 multiple non-Smad mediated intracellular signaling pathways such as MAP kinase
67 pathways and phosphatidylinositol-3-kinase/AKT pathways[13, 14]. These non-Smad
68 (noncanonical) TGFß signaling pathways are equally critical for driving some specific
69 cellular processes (e.g., cell proliferation, cell survival, endothelial/epithelial
70 mesenchymal transition)[13, 14]. During cardiovascular development, unsurprisingly, TGFß
71 signaling is implicated in most morphological events including cardiac lineage
72 specification, cardiac looping, valvogenesis, and cardiomyogenesis[15]. The TGFß family
73 includes TGFß1, TGFß2, and TGFß3. Although TGFß1, TGFß2 and TGFß3 are
74 abundantly expressed in the developing endocardium and epicardium, it appears that
75 they do not perform redundant functions: individual knockout results in different
76 phenotypes[15]. For instance, global knockout of either *Tgfß2* or *Tgfß3* result in early
77 perinatal lethality, presenting hypoplastic hearts with thin myocardium[16, 17], suggesting
78 that they play critical roles for myocardial growth. In contrast, global knockout of *Tgfß1*
79 lead to partial embryonic lethality with survivors appearing phenotypically normal in first
80 the two weeks of life[18]. Nonetheless, it is poorly understood how the expression of TGFß
81 ligands are regulated in the early developing heart.
82 Epigenetic modulators such as histone deacetylases (HDACs) are critical for early heart
83 development as key regulators of regulating gene expresison[19, 20]. There are 18 known
84 human HDACs, which can be subdivided into four classes based on their function and
85 DNA sequence similarity. Class I HDACs include HDAC1, HDAC2, HDAC3, and HDAC8,
86 and are predominantly nuclear and ubiquitously expressed[21]. Although class I HDACs

87 have high degree of homology, global knockout of each causes early embryonic lethality[19],
88 suggesting distinct roles during early heart development. Global deletion of *Hdac3* leads
89 to early embryonic lethality at gastrulation[22]. In the developing heart, lack of *Hdac3* in
90 cardiac progenitors disrupts secondary heart field development[23], lymphovenous valve
91 morphogenesis[24], and CM lineage specification[25]. Recently, we reported that HDAC3 in
92 the developing epicardium plays a critical role in supporting compact myocardial wall
93 expansion[26]. It is unclear whether or how HDAC3 in the developing endocardium impacts
94 myocardial trabeculation.
95 In the current study, we investigated the role of HDAC3 in the developing endocardium
96 during early heart development.

97 **Results**

98 **Endothelial/Endocardial cell specific deletion of *Hdac3* results in embryonic**
99 **lethality and hypotrabeculation.**

100 To study the role of HDAC3 in the cardiac endothelium during early heart development,
101 *Hdac3* was specifically deleted in the endothelial cells using *Tie2-Cre*[27], while its
102 expression in other cells including CMs remains intact (Supplemental Figure 1). Note:
103 since *Tie2-Cre* is transiently expressed in oocytes[28], the mating scheme was always
104 *Hdac3*$^{f/+}$*; Tie2-Cre/+* (♂) and *Hdac3*$^{f/f}$ (♀). By recovering the progenies at a series of
105 embryonic and postnatal stages, we identified that *Hdac3* KO in the developing
106 endothelium resulted in early embryonic lethality starting at E12.5 (Supplemental Table
107 1). To investigate the potential cause of early embryonic lethality, we performed
108 histological analyses. Interestingly, in Tie2 endothelial *Hdac3* KO embryos (*Hdac3*^{tko}),
109 there was no noticeable phenotype in the various endothelial cell derived tissue where
110 the Tie2-lineage contributes, such as endocardium (Figure 1, Supplemental Figure 2) and
111 blood vessels (Supplemental Figure 3), given that *Tie2-Cre* is active in all endothelial cells
112 in the body[29]. In contrast, there were myocardial defects in *Hdac3*^{tko} embryos starting at
113 E11.5: *Hdac3*^{tko} trabeculae appeared to be significantly sparser and shorter as compared
114 to the thick and long webbing like trabecular network in littermate control hearts
115 (Supplemental Figure 2). This cardiac phenotype in *Hdac3*^{tko} mice was more prominent
116 at E12.5 (Figure 1A). The compact layer was also significantly thinner in *Hdac3*^{tko} hearts.
117 To further validate the myocardial trabecular phenotype in endothelial *Hdac3* deleted
118 hearts, we specifically deleted *Hdac3* in the endocardium using *Nfatc1*$^{Cre/+}$, endocardial
119 specific Cre[30], which also resulted in embryonic lethality (Supplemental Table 2).

120 *Hdac3*^{nko} (*Hdac3*$^{f/f}$*; Nfatc1*$^{Cre/+}$) hearts presented a similar cardiac phenotype, albeit at a
121 later stage (E14.5): smaller and sparser trabeculae, thinner compact wall (Supplemental
122 Figure 4). This is consistent with the achievement of late deletion of *Hdac3* in the
123 endocardium by *Nfatc1*$^{Cre/+}$ (Supplemental Figure 4). Nonetheless, these results confirm
124 that the cardiac phenotypes resulting from *Tie2* endothelial *Hdac3* deletion are primarily
125 from the endocardium, and not secondary to another endothelium (e.g., vascular).
126 *Hdac3*^{tko} embryos were used for all subsequent mechanistic studies.
127
128 **Endothelial *Hdac3* knockout hearts display decreased trabecular CM proliferation.**
129 Next, we investigated whether altered cell proliferation and/or apoptosis contribute to the
130 hypotrabeculation phenotypes in *Hdac3*^{tko} hearts. At E11.5, the percentage of either p-
131 H3+ or BrdU+ CMs is significantly lower in *Hdac3*^{tko} trabecular and compact myocardium
132 as compared to littermate control hearts (Figure 1B). This finding is consistent with the
133 hypoplastic cardiac phenotypes seen in *Hdac3*^{tko} hearts (Figure 1A). In contrast, there
134 was no significant difference in cell apoptosis between *Hdac3*^{tko} hearts and littermate
135 control hearts (Supplemental Figure 5). Decreased CM proliferation of *Hdac3*^{tko} hearts
136 may result from disrupted communication from the endocardium to the trabecular
137 myocardium. We performed single cell RNA-sequencing (scRNA-seq) on E11.5 *Hdac3*^{tko}
138 hearts and littermate control hearts (Figure 2A). We obtained high-quality scRNA-seq
139 profiles for 23,468 and 25,547 cells from 4 *Hdac3*^{tko} (*Hdac3*$^{f/f}$*; Tie2-Cre/+; R26*$^{eYFP/+}$) and
140 4 control (3 of *Hdac3*$^{f/+}$*; Tie2-Cre/+; R26*$^{eYFP/+}$ and 1 of *Hdac3*$^{f/+}$*; Tie2-Cre/+*) heart single
141 cell suspensions, respectively. Unsupervised clustering successfully separated 6 distinct
142 clusters including endocardial cells and CMs in these samples (Figure 2B and

143 Supplemental Figure 6). Referring to a recent transcriptome profiling methodology for
144 clustering embryonic CMs[31], we re-clustered CMs into “trabecular” and “compact” clusters
145 based on the overall scores after applying a few known trabecular and compact markers
146 (trabecular: *Bmp10*, *Nppa* and *Thbs4*; compact: *Hey2*, *Mycn* and *Tnnt1*) (Supplemental
147 Figure 7A and Figure 2C). Among them, *Bmp10*+ CMs nicely represent the trabecular
148 cluster (Figure 2C), and thus we focused on this population for subsequent analyses since
149 *Hdac3*^{tko} hearts mainly display hypotrabeculation phenotypes (Figure 1). Overall, the total
150 number of *Bmp10*+ trabecular CMs were not significantly different between *Hdac3*^{tko} and
151 littermate control hearts (Supplemental Figure 7B). Note: 10,000 cells/sample was
152 sequenced. Next, we performed differential gene expression (DGE) analyses on *Hdac3*^{tko}
153 and littermate control trabecular clusters. We found that the expression of eukaryotic
154 translation elongation factor 1 alpha 2 (*Eef1a2*) and early growth response-1 (*Egr-1*) are
155 significantly down regulated in *Hdac3*^{tko} trabeculae as compared to control trabeculae
156 (Figure 2D). *Eef1a2* and *Egr1* are known to be critical for cell growth[32-34]. These findings
157 are consistent with reduced proliferation index seen in *Hdac3*^{tko} hearts (Figure 1B),
158 suggesting myocardial growth retardation account for the hypotrabeculation phenotypes
159 in *Hdac3*^{tko} hearts.
160

161 **Endothelial HDAC3 induces ECM gene expression.**

162 Among all scRNA-seq samples, 7 of them carried *R26*$^{eYFP/+}$ reporters (3 CTL and 4
163 *Hdac3*^{tko}). This enabled us to perform a lineage specific analysis. In the single cell
164 suspension, 8.6% cells in CTL hearts and 11.2% cells in *Hdac3*^{tko} hearts were YFP+
165 (Supplemental Figure 8A). As expected, the expression of *Hdac3* in YFP+ populations in

166 *Hdac3*^{tko} hearts was significantly decreased compared to YFP+ populations in CTL hearts
167 (Supplemental Figure 8B). During early heart development, endothelial progenitors can
168 also give rise to fibroblasts/mesenchymal cells through endothelial to mesenchymal
169 transition[6, 35]. As expected, YFP+ cells (Tie2 lineage) were primarily CECs with a minority
170 of fibroblasts (Figure 2E). Also, as expected, *Hdac3* expression was absent in *Hdac3*^{tko}
171 YFP+ cells. Subsequent DGE analysis did not reveal significant gene expression
172 differences between *Hdac3*^{tko} and control fibroblasts (Figure 2E). Instead, in CEC clusters,
173 we found that the expression of genes regulating cellular component organization was
174 highly enriched in the control YFP+ CEC cluster (Figure 2F). In particular, the expression
175 of ECM associated genes, including *Col13a1, Col1a2, Tgfbi, Timp2, Col26a1, Col3a1,*
176 *Col4a5*, *Timp3*, and *P4ha3*, was significantly reduced in *Hdac3*^{tko} YFP+ CEC cluster as
177 compared to control YFP+ CEC cluster (Figure 2G). *Col1a1, Col1a2, Col2a1*, and *Col3a1*
178 and *P4ha3* DGE was further validated in *Hdac3*^{tko} and control heart lysates by qRT-PCR
179 (Figure 2H). These results suggest that cardiac endothelial HDAC3 induces the
180 expression of ECM associated genes, which are critical for CM proliferation and
181 trabeculation growth (Figure 2I).
182
183 **Cardiac endothelial HDAC3 induces *Tgfβ3* in driving CM proliferation.**
184 Trabeculation and ECM remodeling are coordinated during early heart development, and
185 both processes are regulated by growth signaling[36]. To better identify potential growth
186 signaling pathways regulated by HDAC3 in the endocardium, we used a mouse cardiac
187 endothelial cell (MCEC) line[37]. Using CRISPR-Cas9 gene editing technology and the
188 same set of gRNAs we have recently used[26], we successfully knocked out *Hdac3* in the

189 MCECs (Figure 3A). *Hdac3* KO MCECs grew slower than *Hdac3* empty vector (EV)
190 control MCECs. To determine whether the secretome from *Hdac3* KO endothelial cells is
191 competent to induce CM proliferation, we treated cultured primary embryonic CMs
192 isolated from E13.5 *Tnnt2*$^{nGFP/+}$[38] hearts with supernatant from either *Hdac3* KO MCECs
193 or *Hdac3* EV MCECs, respectively. *Hdac3* KO supernatant treatment resulted in
194 significant decrease of the percentage of Ki67+ CMs and the total number of CMs, as
195 compared to *Hdac3* EV supernatant treatment (Figure 3B). These results suggest that
196 growth signals derived from CECs required to support CM proliferation may be
197 inadequate/deficient in *Hdac3* KO MCECs. To unbiasedly search for such growth signals,
198 we performed bulk RNA-Seq analyses on *Hdac3* KO and EV MCECs; we identified 484
199 downregulated and 239 upregulated genes. Gene ontology pathway analyses revealed
200 that a number of endocardium-initiated signaling pathways were significantly
201 downregulated in *Hdac3* KO MCECs (Supplemental Figure 9A). Through DGE analysis,
202 we found that growth factors including *Igf1, Tgfβ3, Tgfβ2, Tgfβ1, Igf1, Cxcl12, Nrg1 and*
203 *Vegfβ* were significantly downregulated in *Hdac3* KO MCECs (Supplemental Figure 9B).
204 We attempted to validate these results at the protein level by western blot. Surprisingly,
205 we found that only TGFβ3 protein expression was significantly decreased in *Hdac3* KO
206 MCECs as compared to *Hdac3* EV MCECs (Supplemental Figure 9C), and thus we chose
207 TGFβ3 to pursue further. Interestingly, TGFβ3 was also significantly decreased when the
208 deacetylase activity of HDAC3 was inhibited by RGFP966 (a HDAC3 selective inhibitor)
209 treatment (Figure 3C and Supplemental Figure 9D). To assess *Tgfβ3* expression in E11.5
210 CECs, we sorted Tie2-derived population from *Hdac3*^{tko} (*Hdac3*$^{f/f}$*; Tie2-Cre/+; R26*$^{eYFP/+}$)
211 and CTL (*Hdac3*$^{f/+}$*; Tie2-Cre/+; R26*$^{eYFP/+}$) hearts by performing fluorescence activated

212 cell sorting on YFP signal (Supplemental Figure 10). We found that *Tgfβ3* mRNA level
213 was also significantly downregulated in E11.5 *Hdac3* KO CECs compared to littermate
214 CTL CECs (Figure 3D). TGFβ3 downregulation in E11.5 *Hdac3*^{tko} hearts was further
215 validated at the protein level by western blot (Figure 3E). Next, we determined whether
216 TGFβ3 deficiency in *Hdac3* KO MCECs contributed to the CM proliferation deficit
217 following *Hdac3* KO supernatant treatment. First, we quantified TGFβ3 and found that it
218 was significantly decreased in the supernatants from *Hdac3* KO MCECs compared to that
219 from *Hdac3* EV MCECs (Figure 3F). To determine whether TGFβ3 is an essential
220 secretory component of MCEC supernatants in stimulating CM proliferation, we
221 generated *Tgfβ3* KO MCECs using CRISPR-Cas9 gene editing technology
222 (Supplemental Figure 11A). We found that *Tgfβ3* KO significantly decreased the capacity
223 of MCEC supernatants to induce CM proliferation (percentage of Ki67+GFP+/GFP+ CMs)
224 compared to CTL MCEC supernatant (Supplemental Figure 11B). Further, we found that
225 *Tgfβ3* KO significantly compromised the capacity of MCEC supernatants in supporting
226 myocardial trabeculation and compaction when treating *ex vivo* cultured E11.5 wildtype
227 hearts with *Tgfβ3* KO MCEC supernatants as compared to control MCEC supernatants
228 (Supplemental Figure 11C). These results altogether suggest that endocardial TGFβ3 is
229 critical for myocardial growth. Next, we evaluated CM proliferation after we supplemented
230 *Hdac3* KO supernatants with recombinant mouse TGFβ3 protein. Strikingly, TGFβ3
231 supplementation successfully rescued CM proliferation defects by *Hdac3* KO supernatant
232 treatment (Figure 3G). Further, we found that TGFβ3 supplementation also rescued
233 myocardial growth deficit in *ex vivo* cultured E11.5 *Hdac3*^{tko} hearts (Supplemental Figure

234 12). These results suggest that cardiac endothelial HDAC3 supports myocardial growth
235 by inducing *Tgfβ3* expression.

236 **Cardiac endothelial HDAC3 induces *Tgfβ3* expression through repressing**
237 **microRNA (miR)-129-5p.**

238 Recently, we reported that HDAC3 regulates growth factors by modulating the miR
239 pathway in the developing epicardium[26]. To identify the potential HDAC3 downstream
240 miR targets in CECs, we performed miR sequencing in *Hdac3* KO and EV MCECs.
241 Through DGE analyses, we found that 5 miRs were significantly upregulated in *Hdac3*
242 KO MCECs (Figure 4A) (cutoff threshold: Log2 fold change greater than 1.5 and adjusted
243 $P<0.01$). To identify which miR(s) may regulate *Tgfβ3* expression, we treated MCECs
244 with mimics of each of the 5 miRs and found that treatment with miR-129-5p mimics
245 significantly inhibited the expression of *Tgfβ3* (Figure 4B). This finding was validated by
246 western blot (Figure 4C). We further validated the upregulation of miR-129-5p in both
247 *Hdac3* KO MCECs and E11.5 $Hdac3^{tko}$ hearts (Figure 4D and 4E). Interestingly, miR-
248 129-5p was similarly significantly upregulated when the deacetylase activity of HDAC3 is
249 inhibited by RGFP966 treatment (Figure 4D), suggesting that the inhibition of miR-129-
250 5p expression by HDAC3 is deacetylase dependent. To determine whether miR-129-5p
251 upregulation in MCECs has potential impact on myocardial growth, we treated cultured
252 $Tnnt2^{nGFP/+}$[38] CMs or cultured whole E11.5 wildtype hearts with supernatants from
253 MCECs transfected with either miR-129-5p mimics or scramble RNAs. We found that
254 miR-129-5p supernatant treatment significantly decreased its capacity to induce CM
255 proliferation and myocardial growth (Supplemental Figure 13). Lastly, to determine
256 whether HDAC3 induces *Tgfβ3* expression through repressing miR-129-5p, we knocked

257 down miR-129-5p by miRZip lentivirus in *Hdac3* KO MCECs. Remarkably, miR-129-5p
258 knockdown significantly restored the TGFβ3 expression in *Hdac3* KO MCECs (Figure 4G).
259 Further, the supernatants from miR-129-5p knockdown *Hdac3* KO MCECs significantly
260 restored the CM proliferation promoting capacity from *Hdac3* KO MCEC supernatants
261 (Figure 4H). These results suggest that HDAC3 promotes the expression of TGFβ3
262 through repressing miR-129 in supporting trabecular myocardial growth (Figure 4I).

263 **Discussion**

264 Myocardial growth/expansion, one of the most critical cardiac developmental events, is
265 accompanied by two separate but closely associated processes: compaction and
266 trabeculation. Many forms of congenital heart disease are associated with abnormal
267 cardiac trabeculation and compaction[2, 3]. For proper myocardial development, besides
268 cardiomyocytes, the surrounding non-cardiomyocytes including endocardial cells can
269 influence myocardial growth by sending growth signals to the neighboring myocardia[39],
270 as well as secreting ECM proteins that serve as signal transmission media[2, 40]

271 Epigenetic regulation can define a tissue-specific and developmental stage-specific
272 transcription network during early heart development[41, 42], mainly achieved by
273 posttranslational modifications of histones, around which DNA winds. There are several
274 different types of histone modifications (e.g., methylation/demethylation,
275 acetylation/deacetylation, phosphorylation/dephosphorylation, ubiquitination/
276 deubiquitination). By alternating between any of these states, the associated genes can
277 be dynamically poised to be transcriptionally active/repressed. Histone deacetylases
278 (HDACs) are family of enzymes that remove acetyl groups from a lysine residue on a
279 histone, allowing the histones to wrap the DNA more tightly to repress gene expression.
280 Class I HDACs, includes HDAC3, are widely expressed, but play specific roles during
281 early embryogenesis and organogenesis[19]. Mesodermal or global knockout of *Hdac3*
282 results in myogenic defects and early embryonic lethality[22, 43]. Interestingly, specific
283 deletion of *Hdac3* in the myocardium does not generate cardiac morphogenic phenotypes
284 during early heart development, but rather compromises cardiac function at later
285 postnatal stages[43, 44]. These early findings suggest that the function of HDAC3 in

286 nonmyocyte compartments may be critical for early cardiac morphogenesis and
287 myocardial development. Our recent work demonstrated that epicardial HDAC3 is critical
288 for driving myocardial compact wall expansion[26]. Our current study suggests that
289 endocardial HDAC3 is important for myocardial trabeculation: endothelial/endocardial
290 deletion of *Hdac3* resulted in hypotrabeculation (Figure 1 and Supplemental Figure 4).
291 We note that *Tie2-Cre* turns on around E8.0-8.5 in all endothelial cells[29], whereas
292 *Nfatc1*$^{Cre/+}$ is active around E9.5 only in endocardial cells[30] and only achieves efficient
293 *Hdac3* deletion by E14.5 likely due to inefficient IRES-mediated Cre transcription[45]
294 (Supplemental Figure 4). Nonetheless, these two deletion models generated similar
295 cardiac phenotypes of hypotrabeculation, although we did observe differences in the
296 severity of the myocardial phenotypes and time of lethality, which we attribute to the
297 different temporal and spatial activities and/or efficiencies of these two Cres. We also
298 observed that both E12.5 *Hdac3*^{tko} and E14.5 *Hdac3*^{nko} hearts exhibited thin compact wall
299 phenotype. This is likely attributable to *Hdac3* deficiency in the subepicardial endothelial
300 population which form coronary arteries invading and supporting compact wall[46]. This late
301 thin compact wall phenotype is also consistent with the similar phenotype resulted from
302 epicardial deletion of *Hdac3*[26]. An earlier report of conditional deletion of *Hdac3* in
303 endothelial cells using a different Tie2-Cre driver primarily targeting hemogenic
304 endothelial cells[27] resulted in mid-gestational lethality (E14.5) presenting predominantly
305 a lymphovenous and lymphatic valve malformation phenotype[47]. However, it is unknown
306 what phenotypes were present in the myocardium in that study as none were reported.
307 Nonetheless, we deemed it inapplicable to evaluate potential lymphatic valve phenotypes
308 in our pan-endothelial *Hdac3* KO embryos since these mice died around E12.5

309 (Supplemental Table 1), while lymphovenous and lymphatic valve formation starts at
310 E13.5[48]. However, it is interesting to note that the role of HDAC1 and HDAC2 in the
311 developing endocardium appears to be dispensable, as deletion of either *Hdac1* or *Hdac2*
312 by Tie2-Cre do not elicit apparent cardiac phenotypes[24]. These results suggest that
313 HDAC3 plays distinctive roles from HDAC1 and HDAC2, although they share high
314 homology and are grouped in the same HDAC subfamily[19].
315 TGFß signaling is involved in many processes during early heart development such as
316 ECM production, endothelial to mesenchymal transition, and myogenesis[11, 49-51].
317 Specifically, TGFß signaling plays a critical role during early cardiac myocardial
318 development[52-55]. For instance, knockout of either TGFß2 or TGFß3 results in hypoplastic
319 ventricular myocardium[15], while TGFß1 is reported to inhibit CM proliferation[55, 56],
320 suggesting the complexity and specificity of TGFß isoforms during early heart
321 development. In the current study, we found that TGFß3 expression was significantly
322 decreased in *Hdac3* deleted endocardium, and TGFß3 treatment vigorously stimulated
323 CM proliferation (Figure 3). Interestingly, inhibition of deacetylase activity of HDAC3 alone
324 significantly decreased TGFß3 expression. Further, supplementation of TGFß3 to cardiac
325 endothelial Hdac3 KO secretome significantly rescued CM proliferation and myocardial
326 growth defect (Figure 3), suggesting that cardiac endothelial HDAC3 supports
327 trabeculation through inducing TGFß3 in a deacetylase dependent manner. Interestingly,
328 HDAC3 is also reported to inhibit TGFß1 expression in the second heart field
329 development in a deacetylase independent manner[23], whereas HDAC3 deteriorates
330 colorectal cancer progression by inducing TGFß1 through inhibiting miR-296[57]. These

331 divergent findings illustrate that HDAC3 can either promote or inhibit TGFß signaling
332 pathway through different molecular mechanisms in a tissue/cell dependent manner.
333 Besides functioning as growth signals to cardiomyocytes, TGFß signaling is
334 predominantly known for its induction on ECMs[50, 58]. During early heart development,
335 ECM is mainly secreted from endocardium and mediates signal transduction from
336 endocardium to myocardium supporting trabeculation[57]. Our scRNA-Seq data revealed
337 that ECM is significantly down regulated in *Hdac3* endothelial KO hearts (Figure 2).
338 P4ha3, a major enzyme for collagen synthesis[59] and a TGFß downstream target[60], was
339 also significantly decreased in *Hdac3* endothelial knockout hearts (Figure 2). These
340 results suggest that ECM downregulation may be secondary to decreased TGFß
341 signaling to contribute to the hypotrabeculation phenotypes in *Hdac3*
342 endothelial/endocardial knockout hearts.
343 We identified that HDAC3 suppresses miR-129-5p in inducing TGFß3 (Figure 4). miR-
344 129-5p plays important roles in cancer by either promoting or inhibiting tumorigenesis
345 through regulating a variety of downstream targets and pathways[61, 62]. Several studies
346 have shown that miR-129-5p protects adult hearts from ischemia/reperfusion injuries[63,
347 64], while another study demonstrated that treating cultured H9c2 cardiomyocytes with
348 HDAC pan-inhibitor Trichostatin A results in decreased cardiomyocyte proliferation with
349 enhanced miR-129-5p expression[65]. This is consistent with our current findings in the
350 developing endocardium (Figure 4). In our recent study, we found that HDAC3 induces
351 the expression of IGF2 and FGF9 by suppressing miR-322/503 in the developing
352 epicardium[26]. Again, these findings altogether suggest that HDAC3 can induce different

353 sets of growth signals by switching their downstream miR targets in a tissue/cell context
354 dependent manner.
355 In summary, our current study demonstrates that endocardial HDAC3 promotes
356 myocardial trabeculation by inducing TGFß signaling through repressing miR-129-5p
357 during early heart development. This finding, along with others, exemplifies the
358 importance of endocardial signaling for driving myocardial morphogenesis, and thus
359 provides new insights on the pathogenesis of congenital heart disease. The dual
360 epigenetic inhibition mechanism may be leveraged in some other contexts such as adult
361 heart repair/regeneration.

362 **Methods**

363 ***Mice***

364 *Hdac3*$^{flox/+}$, *Tie2-Cre*, *Nfatc1*$^{Cre/+}$, *R26*^{eYFP} and *Tnnt2*$^{nGFP/+}$ mice were previously
365 described[27, 30, 38, 66, 67]. B6.Cg-Tg(*Tek-cre*)12Flv/J (abbreviated as *Tie2-Cre* in this
366 manuscript), *Hdac3*$^{flox/+}$, and *R26*^{eYFP} mice are available at the Jackson Laboratory (Stock
367 numbers: #004128, #024119 and #006148, respectively). All animal protocols were
368 approved by the Nationwide Children's Institutional Animal Care and Use Committee
369 (IACUC #AR22-00194).

370

371 ***Histology and immunofluorescence staining***

372 All embryo specimens were fixed in 4% paraformaldehyde overnight, dehydrated through
373 an ethanol series, paraffin embedded, and sectioned (6-7μm). Primary antibodies (Major
374 Resources Table) were incubated at 4°C overnight and secondary antibodies (Alexa 488
375 or Alexa 555, Thermo Fisher Scientific, Waltham, MA) were incubated at room
376 temperature for one hour. Stained slides were imaged on a Zeiss LSM 710 confocal
377 Microscope or a Leica DM6 fluorescence microscope. Epifluorescence and gross images
378 of embryos were imaged on a Leica M205 FCA stereo fluorescence microscope. The
379 number of phosphor-Histone 3 (p-H3)+ cells, Bromodeoxyuridine (BrdU)+ cells, and
380 TUNEL+ cells was quantified using ImageJ software.

381

382 ***Embryonic cardiomyocyte culture and proliferation assessment***

383 E13.5 ventricular cardiomyocytes were isolated from dissected embryonic hearts and
384 cultured as previously described[68]. To assess cell proliferation, cardiomyocytes were

385 fixed with 4% paraformaldehyde and stained with Ki67 or p-H3 antibody followed by Alexa
386 594-conjugated secondary antibody (Thermo Fisher Scientific, Waltham, MA). The
387 immunostaining was visualized and imaged on a Keyence BZ-X800 microscope. The
388 percentages of Ki67+GFP+/GFP+, p-H3+GFP+/GFP+ and total number of GFP+
389 cardiomyocytes were quantified using ImageJ software.

390

391 ***Endothelial cell culture, transient transfection, lentiviral infection, and luciferase***
392 ***assay***

393 Mouse cardiac endothelial cells (MCECs) were purchased from Cedarlane Labs
394 (Catalogue #CLU510, Burlington, NC). MCECs were cultured in 10% fetal bovine serum
395 (FBS) supplemented DMEM at 37°C in a humidified incubator with 5% CO_2. To generate
396 stable *Hdac3* KO MCECs, as previously described[26], we cloned *Hdac3* sgRNA into
397 lentiCRISPR v2 vector (Addgene #52961; Watertown, MA). Seventy-percent confluent
398 Lenti-X™ 293T cells (Takara Bio USA, Inc., Mountain View, CA) were transfected with
399 *Hdac3* lentiviral plasmids (*Hdac3* KO or empty vector control [EV])[26], *Tgfβ3* lentiviral
400 plasmids (*Tgfβ3* KO or empty vector control [EV]) were purchased from VectorBuilder,
401 PsPAX2 (Addgene #12260) and PMD2G (Addgene #12259). Seventy-two hours after
402 transfection, supernatants containing lentivirus were collected and filtered through a
403 40μm cell strainer. Mir-129-5p, miR-129b-3p, miR-129b-5p, mir-129-2-3p, miR-708-3p
404 mimics and scramble control mimics were custom-ordered from ThermoFischer Scientific
405 (Waltham, MA). MCECs were transfected with miRNA mimics or control mimics (30 pmol)
406 using Lipofectamine RNAiMAX (Thermo Fisher Scientific, Waltham, MA). 72 hours after
407 miR mimics treatment, supernatants were collected. miRZip anti-miR precursor

408 constructs for miRZip-129-5p and pGreenPuro Scramble Hairpin control constructs were
409 purchased from System Biosciences (Palo Alto, CA), and lentiviruses were generated
410 according to the manufacturer's protocol.
411
412 ***Ex Vivo embryonic heart culture***
413 E11.5 embryonic hearts were dissected in cold PBS, and then cultured in DMEM/F-12
414 media (Thermofisher Scientific, Waltham, MA, #11039021). Embryonic cardiac explants
415 were treated with either TGFß3 recombinant protein (Sigmal Aldrich, Saint Louis, MO,
416 #SRP6552, final concentration: 250 ng/ml), TGFß3 KO MCEC supernatants, miR-129-5p
417 mimics-treated MCEC supernatants and their corresponding control media or control
418 MCEC supernatants for 24 h at 37 °C. Hearts were then fixed in 4% paraformaldehyde
419 overnight at 4 °C and processed for paraffin embedding and sectioning.
420
421 ***Fluorescence activated cell sorting of YFP+ Tie2 derivative cardiac cells***
422 E11.5 hearts were dissected and dissociated with 0.5% trypsin–EDTA into a single cell
423 suspension. Cell suspension was washed with PBS and YFP+ cells were gated using
424 their autofluoresence signal and sorted and using a BD Influx cell sorter (BD Biosciences).
425 The harvested YFP+ cells were used for subsequent gene expression analysis.
426
427 ***RNA isolation, quantitative real-time PCR (qRT-PCR), and bulk RNA-Seq***
428 MCECs and embryonic day (E) 11.5 hearts were used for RNA isolation. E11.5 hearts
429 were microdissected in cold PBS and snap frozen in liquid nitrogen. The RNeasy Plus
430 Mini Kit (QIAGEN, Germantown, MD) was used to extract total RNA, and cDNAs were

431 generated using the Superscript III kit (Thermo Fisher Scientific, Waltham, MA). To detect
432 mRNA, SYBR Green qRT-PCR was performed. PCR primers for genes of interest are
433 listed in Major Resources Table. To perform mature microRNA expression analyses,
434 purified total RNAs were converted to cDNAs using TaqMan™ MicroRNA Reverse
435 Transcription Kit (Catalogue #4366596, Thermo Fisher Scientific). qRT-PCR reactions
436 were run on StepOne Plus Real-Time PCR System (Applied Biosystems, Waltham, MA).
437 The probe sequences for mmu-miR-129-5p and U6 snRNA were purchased from Thermo
438 Fisher Scientific. For bulk RNA and miRNA-Sequencing, samples were prepared
439 following the provider's guidelines (Novogene Corporation Inc, Sacramento, CA) and
440 sequenced on an Illumina NextSeq500 (San Diego, CA). Sequencing reads were aligned
441 to the UCSC mm10 reference genome using tophat2 and bowtie2 in R. Differential
442 expression of transcripts was calculated using the cufflinks suite in R analyses.
443
444 ***Single cell RNA-Sequencing (scRNA-seq)***
445 E11.5 heart tissues were dissected in cold PBS and digested with 0.25% trypsin at 37°C
446 for 15 minutes. Digested cardiac cells were filtered with 70 μm cell strainers to remove
447 remaining clumps. Subsequently, 10,000 live cells were captured with Chromium Next
448 GEM Single Cell 3' Reagent Kits v3.1 (10X Genomics, Pleasanton, CA) following
449 manufacturer's instructions. Briefly, single cells were partitioned into nanoliter-scale Gel
450 Beads-in-emulsion (GEMs) using Chromium Next GEM Chip G in the chromium controller.
451 Immediately following GEM generation, the Gel Bead was dissolved, primers were
452 released, and co-partitioned cell was lysed, and its mRNA were reverse transcribed into
453 barcoded cDNA. After further cleanup and amplification, the cDNA was enzymatically

454 fragmented and amplified via PCR to generate sufficient mass for library construction.
455 After end repair, A-tailing, adaptor ligation and sample index PCR, the library comprised
456 constructs containing the sample index, UMI sequences, barcode sequences, and
457 Illumina standard sequencing primers P5 and P7 at both ends. The library was sequenced
458 with Illumina NextSeq S4 platform to a sequencing depth of 140-270 million reads per
459 sample. Reads were aligned to the Ensembl 104 mouse reference genome including the
460 sequence for eYFP as a separate contig using STARsolo (version 2.7.10b)[69]. The
461 resulting count tables (cells x genes) were converted into Annotated Data (anndata)
462 format for analysis in Python. For quality control, all cells with less than 1500 or more than
463 9000 genes expressed were excluded. Additionally, cell doublets were filtered out using
464 the Scrublet method[70]. Gene counts were normalized per cell to a total target sum and
465 transformed using log1p. Highly variable genes were identified using the Seurat method[71]
466 and these genes were utilized for dimension reduction with PCA. Finally, cell embedding
467 was performed with the UMAP algorithm (umap-learn version 0.5.3) and cells were
468 clustered using leiden (leidenalg version 0.9.1) with resolution 0.2. Scoring of trabecular
469 and compact CM subtypes was performed using 'score_genes' and differentially
470 expressed genes between groups were obtained using 'rank_genes_groups', both
471 methods from the SCANPY package[72].
472
473 ***Western blotting***
474 Cell or tissue lysates were prepared in lysis buffer (20 mM Tris-HCl [pH 7.5], 15 mM NaCl,
475 1 mM Na_2EDTA, 1 mM EGTA, 1% Triton X-100, 1 μg/ml leupeptin, 2.5 mM sodium
476 pyrophosphate, 1 mM Na_3VO_4, and 1 mM β-glycerophosphate) with protease inhibitor

477 cocktail (Roche, Indianapolis, IN) and 1 mM phenylmethylsulfonyl fluoride. Protein
478 samples were resolved on 4–12% SDS-PAGE acrylamide gels before transferring to
479 polyvinylidene fluoride membranes. Primary antibodies were visualized by
480 chemiluminescence using HRP-conjugated secondary antibodies. Antibodies are listed
481 in Major Resources Table. Western blots were normalized to loading controls and
482 densitometric analysis was performed using Image J software.
483
484 ***Statistical analysis***
485 All experiments were independently repeated at least three times, and the number of
486 samples (n) is stated in figure legends. Results are reported as the mean ± SD. For
487 statistical analyses, normal distribution of data was assessed by Shapiro-Wilk's test
488 (when n≥6). For data with small sample size (n<6), non-parametric tests were applied.
489 For parametric data with normal distribution, the statistical significance of the difference
490 between means was assessed using the unpaired two tailed Student's t-test between two
491 groups and the Tukey or Dunnett post hoc test for one-way ANOVA. For non-parametric
492 data or data with small sample size (n<6), the Mann-Whitney U test and Kruskal-Wallis
493 test for one-way ANOVA followed by the Dunn post hoc test were performed for
494 comparisons between two groups. Specific statistical tests are stated in figure legends.
495 RNA-seq data were background-corrected, variance-stabilized, normalized, and count
496 matrix extracted through quality control using lumi package for the R programming
497 language (http://bioconductor.org/packages/release/bioc/html/lumi.html). Differential
498 expression analysis was performed using DESeq2 R package
499 (https://bioconductor.org/packages/release/bioc/html/DESeq2. html). The resulting *p*-

500 values were adjusted using the Benjamini and Hochberg's approach for controlling the
501 False Discovery Rate (FDR)[73]. Genes or miRs with an adjusted *p*-value<0.05 found by
502 DESeq2 were assigned as differentially expressed. Gene ontology (GO) enrichment
503 analyses were performed using the Database for Annotation, Visualization and Integrated
504 Discovery (DAVID) bioinformatics resources (https://david.ncifcrf.gov/). For relative gene
505 expression analysis of qRT-PCR data, the expression of a gene of interest relative to an
506 internal loading control gene was calculated using the comparative CT method (-ΔΔCT)[74].
507 The relative protein expression on western blots was quantified by densitometry, Fold
508 changes for relative gene or protein expression were derived through division of values
509 in the experimental group by the mean values from the control group. *P*-value<0.05 was
510 considered statistically significant. All statistical analyses were performed using
511 GraphPad Prism 8 (GraphPad Prism software, Inc). The images with the value closest to
512 the mean value were selected as representative images.
513

514 **Data Availability**

515 All data associated with this study are present in the main text or the supplementary
516 materials. The scRNA-seq, RNA-seq and miRNA-seq data generated in this study have
517 been deposited in the GEO database under accession code GSE229661. All raw data
518 are available from the authors upon reasonable request.

519

520 **References:**

521 1. Zaidi S and Brueckner M. Genetics and Genomics of Congenital Heart Disease.
522 *Circulation research*. 2017;120:923-940.

523 2. Qu X, Harmelink C and Baldwin HS. Endocardial-Myocardial Interactions During Early
524 Cardiac Differentiation and Trabeculation. *Front Cardiovasc Med*. 2022;9:857581.

525 3. Wu M. Mechanisms of Trabecular Formation and Specification During Cardiogenesis.
526 *Pediatric cardiology*. 2018;39:1082-1089.

527 4. Lin W and Li D. Zinc and Zinc Transporters: Novel Regulators of Ventricular Myocardial
528 Development. *Pediatric cardiology*. 2018;39:1042-1051.

529 5. Zhang W, Chen H, Qu X, Chang CP and Shou W. Molecular mechanism of ventricular
530 trabeculation/compaction and the pathogenesis of the left ventricular noncompaction
531 cardiomyopathy (LVNC). *American journal of medical genetics Part C, Seminars in medical*
532 *genetics*. 2013;163C:144-56.

533 6. Zhang H, Lui KO and Zhou B. Endocardial Cell Plasticity in Cardiac Development,
534 Diseases and Regeneration. *Circulation research*. 2018;122:774-789.

535 7. Andries LJ, Sys SU and Brutsaert DL. Morphoregulatory interactions of endocardial
536 endothelium and extracellular material in the heart. *Herz*. 1995;20:135-45.

537 8. Camenisch TD, Spicer AP, Brehm-Gibson T, Biesterfeldt J, Augustine ML, Calabro A, Jr.,
538 Kubalak S, Klewer SE and McDonald JA. Disruption of hyaluronan synthase-2 abrogates normal
539 cardiac morphogenesis and hyaluronan-mediated transformation of epithelium to mesenchyme.
540 *J Clin Invest*. 2000;106:349-60.

541 9. Hatano S, Kimata K, Hiraiwa N, Kusakabe M, Isogai Z, Adachi E, Shinomura T and
542 Watanabe H. Versican/PG-M is essential for ventricular septal formation subsequent to cardiac
543 atrioventricular cushion development. *Glycobiology*. 2012;22:1268-77.

544 10. Chen JL, Colgan TD, Walton KL, Gregorevic P and Harrison CA. The TGF-beta Signalling
545 Network in Muscle Development, Adaptation and Disease. *Adv Exp Med Biol*. 2016;900:97-131.

546 11. Sorensen DW and van Berlo JH. The Role of TGF-beta Signaling in Cardiomyocyte
547 Proliferation. *Curr Heart Fail Rep*. 2020;17:225-233.
548 12. Zhang Y and Yang X. The Roles of TGF-beta Signaling in Cerebrovascular Diseases.
549 *Front Cell Dev Biol*. 2020;8:567682.
550 13. Moustakas A and Heldin CH. Non-Smad TGF-beta signals. *J Cell Sci*. 2005;118:3573-84.
551 14. Zhang YE. Non-Smad pathways in TGF-beta signaling. *Cell Res*. 2009;19:128-39.
552 15. Azhar M, Schultz Jel J, Grupp I, Dorn GW, 2nd, Meneton P, Molin DG, Gittenberger-de
553 Groot AC and Doetschman T. Transforming growth factor beta in cardiovascular development
554 and function. *Cytokine Growth Factor Rev*. 2003;14:391-407.
555 16. Koo SH, Cunningham MC, Arabshahi B, Gruss JS and Grant JH, 3rd. The transforming
556 growth factor-beta 3 knock-out mouse: an animal model for cleft palate. *Plast Reconstr Surg*.
557 2001;108:938-48; discussion 949-51.
558 17. Sanford LP, Ormsby I, Gittenberger-de Groot AC, Sariola H, Friedman R, Boivin GP,
559 Cardell EL and Doetschman T. TGFbeta2 knockout mice have multiple developmental defects
560 that are non-overlapping with other TGFbeta knockout phenotypes. *Development*.
561 1997;124:2659-70.
562 18. Kulkarni AB and Karlsson S. Transforming growth factor-beta 1 knockout mice. A mutation
563 in one cytokine gene causes a dramatic inflammatory disease. *Am J Pathol*. 1993;143:3-9.
564 19. Haberland M, Montgomery RL and Olson EN. The many roles of histone deacetylases in
565 development and physiology: implications for disease and therapy. *Nature reviews Genetics*.
566 2009;10:32-42.
567 20. Dsilva P, Pai P, Shetty MG and Babitha KS. The role of histone deacetylases in embryonic
568 development. *Mol Reprod Dev*. 2023;90:14-26.
569 21. Wang Z, Zhao YT and Zhao TC. Histone deacetylases in modulating cardiac disease and
570 their clinical translational and therapeutic implications. *Exp Biol Med (Maywood)*. 2021;246:213-
571 225.

572 22. Bhaskara S, Chyla BJ, Amann JM, Knutson SK, Cortez D, Sun ZW and Hiebert SW.
573 Deletion of histone deacetylase 3 reveals critical roles in S phase progression and DNA damage
574 control. *Mol Cell*. 2008;30:61-72.
575 23. Lewandowski SL, Janardhan HP and Trivedi CM. Histone Deacetylase 3 Coordinates
576 Deacetylase-independent Epigenetic Silencing of Transforming Growth Factor-beta1 (TGF-
577 beta1) to Orchestrate Second Heart Field Development. *The Journal of biological chemistry*.
578 2015;290:27067-27089.
579 24. Janardhan HP, Milstone ZJ, Shin M, Lawson ND, Keaney JF, Jr. and Trivedi CM. Hdac3
580 regulates lymphovenous and lymphatic valve formation. *J Clin Invest*. 2017;127:4193-4206.
581 25. Poleshko A, Shah PP, Gupta M, Babu A, Morley MP, Manderfield LJ, Ifkovits JL, Calderon
582 D, Aghajanian H, Sierra-Pagan JE, Sun Z, Wang Q, Li L, Dubois NC, Morrisey EE, Lazar MA,
583 Smith CL, Epstein JA and Jain R. Genome-Nuclear Lamina Interactions Regulate Cardiac Stem
584 Cell Lineage Restriction. *Cell*. 2017;171:573-587 e14.
585 26. Jang J, Song G, Pettit SM, Li Q, Song X, Cai CL, Kaushal S and Li D. Epicardial HDAC3
586 Promotes Myocardial Growth Through a Novel MicroRNA Pathway. *Circulation research*.
587 2022;131:151-164.
588 27. Koni PA, Joshi SK, Temann UA, Olson D, Burkly L and Flavell RA. Conditional vascular
589 cell adhesion molecule 1 deletion in mice: impaired lymphocyte migration to bone marrow. *The*
590 *Journal of experimental medicine*. 2001;193:741-54.
591 28. de Lange WJ, Halabi CM, Beyer AM and Sigmund CD. Germ line activation of the Tie2
592 and SMMHC promoters causes noncell-specific deletion of floxed alleles. *Physiol Genomics*.
593 2008;35:1-4.
594 29. Kisanuki YY, Hammer RE, Miyazaki J, Williams SC, Richardson JA and Yanagisawa M.
595 Tie2-Cre transgenic mice: a new model for endothelial cell-lineage analysis in vivo. *Dev Biol*.
596 2001;230:230-42.

597 30. Wu B, Zhang Z, Lui W, Chen X, Wang Y, Chamberlain AA, Moreno-Rodriguez RA,
598 Markwald RR, O'Rourke BP, Sharp DJ, Zheng D, Lenz J, Baldwin HS, Chang CP and Zhou B.
599 Endocardial cells form the coronary arteries by angiogenesis through myocardial-endocardial
600 VEGF signaling. *Cell*. 2012;151:1083-96.
601 31. Wu T, Liang Z, Zhang Z, Liu C, Zhang L, Gu Y, Peterson KL, Evans SM, Fu XD and Chen
602 J. PRDM16 Is a Compact Myocardium-Enriched Transcription Factor Required to Maintain
603 Compact Myocardial Cardiomyocyte Identity in Left Ventricle. *Circulation*. 2022;145:586-602.
604 32. Hassan MK, Kumar D, Patel SA and Dixit M. EEF1A2 triggers stronger ERK mediated
605 metastatic program in ER negative breast cancer cells than in ER positive cells. *Life Sci*.
606 2020;262:118553.
607 33. Fish JE, Cantu Gutierrez M, Dang LT, Khyzha N, Chen Z, Veitch S, Cheng HS, Khor M,
608 Antounians L, Njock MS, Boudreau E, Herman AM, Rhyner AM, Ruiz OE, Eisenhoffer GT,
609 Medina-Rivera A, Wilson MD and Wythe JD. Dynamic regulation of VEGF-inducible genes by an
610 ERK/ERG/p300 transcriptional network. *Development*. 2017;144:2428-2444.
611 34. Thornton S, Anand N, Purcell D and Lee J. Not just for housekeeping: protein initiation
612 and elongation factors in cell growth and tumorigenesis. *J Mol Med (Berl)*. 2003;81:536-48.
613 35. Anbara T, Sharifi M and Aboutaleb N. Endothelial to Mesenchymal Transition in the
614 Cardiogenesis and Cardiovascular Diseases. *Curr Cardiol Rev*. 2020;16:306-314.
615 36. Del Monte-Nieto G, Ramialison M, Adam AAS, Wu B, Aharonov A, D'Uva G, Bourke LM,
616 Pitulescu ME, Chen H, de la Pompa JL, Shou W, Adams RH, Harten SK, Tzahor E, Zhou B and
617 Harvey RP. Control of cardiac jelly dynamics by NOTCH1 and NRG1 defines the building plan for
618 trabeculation. *Nature*. 2018;557:439-445.
619 37. Barbieri SS and Weksler BB. Tobacco smoke cooperates with interleukin-1beta to alter
620 beta-catenin trafficking in vascular endothelium resulting in increased permeability and induction
621 of cyclooxygenase-2 expression in vitro and in vivo. *FASEB J*. 2007;21:1831-43.

622 38. Yan J, Zhang L, Sultana N, Oh JG, Wu B, Hajjar RJ, Zhou B and Cai CL. A series of robust
623 genetic indicators for definitive identification of cardiomyocytes. *J Mol Cell Cardiol*. 2016;97:278-
624 85.
625 39. Tian Y and Morrisey EE. Importance of myocyte-nonmyocyte interactions in cardiac
626 development and disease. *Circulation research*. 2012;110:1023-34.
627 40. Silva AC, Pereira C, Fonseca A, Pinto-do OP and Nascimento DS. Bearing My Heart: The
628 Role of Extracellular Matrix on Cardiac Development, Homeostasis, and Injury Response. *Front*
629 *Cell Dev Biol*. 2020;8:621644.
630 41. Paige SL, Thomas S, Stoick-Cooper CL, Wang H, Maves L, Sandstrom R, Pabon L,
631 Reinecke H, Pratt G, Keller G, Moon RT, Stamatoyannopoulos J and Murry CE. A temporal
632 chromatin signature in human embryonic stem cells identifies regulators of cardiac development.
633 *Cell*. 2012;151:221-32.
634 42. Wamstad JA, Alexander JM, Truty RM, Shrikumar A, Li F, Eilertson KE, Ding H, Wylie JN,
635 Pico AR, Capra JA, Erwin G, Kattman SJ, Keller GM, Srivastava D, Levine SS, Pollard KS,
636 Holloway AK, Boyer LA and Bruneau BG. Dynamic and coordinated epigenetic regulation of
637 developmental transitions in the cardiac lineage. *Cell*. 2012;151:206-20.
638 43. Lewandowski SL, Janardhan HP and Trivedi CM. Histone Deacetylase 3 Coordinates
639 Deacetylase-independent Epigenetic Silencing of Transforming Growth Factor-beta1 (TGF-
640 beta1) to Orchestrate Second Heart Field Development. *The Journal of biological chemistry*.
641 2015;290:27067-89.
642 44. Montgomery RL, Potthoff MJ, Haberland M, Qi X, Matsuzaki S, Humphries KM,
643 Richardson JA, Bassel-Duby R and Olson EN. Maintenance of cardiac energy metabolism by
644 histone deacetylase 3 in mice. *J Clin Invest*. 2008;118:3588-97.
645 45. Artap S, Manderfield LJ, Smith CL, Poleshko A, Aghajanian H, See K, Li L, Jain R and
646 Epstein JA. Endocardial Hippo signaling regulates myocardial growth and cardiogenesis. *Dev*
647 *Biol*. 2018;440:22-30.

648 46. Tian X, Hu T, Zhang H, He L, Huang X, Liu Q, Yu W, He L, Yang Z, Zhang Z, Zhong TP,
649 Yang X, Yang Z, Yan Y, Baldini A, Sun Y, Lu J, Schwartz RJ, Evans SM, Gittenberger-de Groot
650 AC, Red-Horse K and Zhou B. Subepicardial endothelial cells invade the embryonic ventricle wall
651 to form coronary arteries. *Cell Res*. 2013;23:1075-90.
652 47. Celikyurt U, Karauzum K, Sahin T, Agacdiken A, Vural A and Ural D. Association between
653 resolution of fragmented QRS and response to cardiac resynchronization therapy. *Ann*
654 *Noninvasive Electrocardiol*. 2015;20:126-31.
655 48. Yang Y and Oliver G. Development of the mammalian lymphatic vasculature. *J Clin Invest*.
656 2014;124:888-97.
657 49. Conway SJ, Doetschman T and Azhar M. The inter-relationship of periostin, TGF beta,
658 and BMP in heart valve development and valvular heart diseases. *ScientificWorldJournal*.
659 2011;11:1509-24.
660 50. Frangogiannis NG. Transforming growth factor-beta in myocardial disease. *Nat Rev*
661 *Cardiol*. 2022;19:435-455.
662 51. Lee JH and Massague J. TGF-beta in developmental and fibrogenic EMTs. *Semin Cancer*
663 *Biol*. 2022;86:136-145.
664 52. Chakrabarti M, Al-Sammarraie N, Gebere MG, Bhattacharya A, Chopra S, Johnson J,
665 Pena EA, Eberth JF, Poelmann RE, Gittenberger-de Groot AC and Azhar M. Transforming
666 Growth Factor Beta3 is Required for Cardiovascular Development. *J Cardiovasc Dev Dis*. 2020;7.
667 53. Dunker N and Krieglstein K. Tgfbeta2 -/- Tgfbeta3 -/- double knockout mice display severe
668 midline fusion defects and early embryonic lethality. *Anat Embryol (Berl)*. 2002;206:73-83.
669 54. Kruithof BP, Kruithof-De-Julio M, Poelmann RE, Gittenberger-De-Groot AC, Gaussin V
670 and Goumans MJ. Remodeling of the myocardium in early trabeculation and cardiac valve
671 formation; a role for TGFbeta2. *Int J Dev Biol*. 2013;57:853-63.
672 55. Kodo K, Ong SG, Jahanbani F, Termglinchan V, Hirono K, InanlooRahatloo K, Ebert AD,
673 Shukla P, Abilez OJ, Churko JM, Karakikes I, Jung G, Ichida F, Wu SM, Snyder MP, Bernstein D

674 and Wu JC. iPSC-derived cardiomyocytes reveal abnormal TGF-beta signalling in left ventricular
675 non-compaction cardiomyopathy. *Nat Cell Biol*. 2016;18:1031-42.
676 56. Engelmann GL, Boehm KD, Birchenall-Roberts MC and Ruscetti FW. Transforming
677 growth factor-beta 1 in heart development. *Mech Dev*. 1992;38:85-97.
678 57. Li J, Hu M, Liu N, Li H, Yu Z, Yan Q, Zhou M, Wang Y, Song Y, Pan G, Liang F and Chen
679 R. HDAC3 deteriorates colorectal cancer progression via microRNA-296-3p/TGIF1/TGFbeta axis.
680 *J Exp Clin Cancer Res*. 2020;39:248.
681 58. Algeciras L, Palanca A, Maestro D, RuizdelRio J and Villar AV. Epigenetic alterations of
682 TGFbeta and its main canonical signaling mediators in the context of cardiac fibrosis. *J Mol Cell*
683 *Cardiol*. 2021;159:38-47.
684 59. Van Den Diepstraten C, Papay K, Bolender Z, Brown A and Pickering JG. Cloning of a
685 novel prolyl 4-hydroxylase subunit expressed in the fibrous cap of human atherosclerotic plaque.
686 *Circulation*. 2003;108:508-11.
687 60. Luo Y, Xu W, Chen H, Warburton D, Dong R, Qian B, Selman M, Gauldie J, Kolb M and
688 Shi W. A novel profibrotic mechanism mediated by TGFbeta-stimulated collagen prolyl
689 hydroxylase expression in fibrotic lung mesenchymal cells. *J Pathol*. 2015;236:384-94.
690 61. Deng B, Tang X and Wang Y. Role of microRNA-129 in cancer and non-cancerous
691 diseases (Review). *Exp Ther Med*. 2021;22:918.
692 62. Xu S, Li W, Wu J, Lu Y, Xie M, Li Y, Zou J, Zeng T and Ling H. The Role of miR-129-5p
693 in Cancer: A Novel Therapeutic Target. *Curr Mol Pharmacol*. 2022;15:647-657.
694 63. Ma R, Chen X, Ma Y, Bai G and Li DS. MiR-129-5p alleviates myocardial injury by
695 targeting suppressor of cytokine signaling 2 after ischemia/reperfusion. *Kaohsiung J Med Sci*.
696 2020;36:599-606.
697 64. Xing J, Liu J, Liu J and Xu Z. miR-129-5p ameliorates ischemia-reperfusion injury by
698 targeting HMGB1 in myocardium. *Gen Physiol Biophys*. 2020;39:461-470.

699 65. Majumdar G and Raghow R. Trichostatin A induces a unique set of microRNAs including
700 miR-129-5p that blocks cyclin-dependent kinase 6 expression and proliferation in H9c2 cardiac
701 myocytes. *Mol Cell Biochem*. 2016;415:39-49.
702 66. Mullican SE, Gaddis CA, Alenghat T, Nair MG, Giacomin PR, Everett LJ, Feng D, Steger
703 DJ, Schug J, Artis D and Lazar MA. Histone deacetylase 3 is an epigenomic brake in macrophage
704 alternative activation. *Genes & development*. 2011;25:2480-8.
705 67. Srinivas S, Watanabe T, Lin CS, William CM, Tanabe Y, Jessell TM and Costantini F. Cre
706 reporter strains produced by targeted insertion of EYFP and ECFP into the ROSA26 locus. *BMC*
707 *Dev Biol*. 2001;1:4.
708 68. Beall MC, Li D and Jang J. Isolation of Embryonic Cardiomyocytes and Cell Proliferation
709 Assay Using Genetically Engineered Reporter Mouse Model. *Bio Protoc*. 2023;13:e4802.
710 69. Dobin A, Davis CA, Schlesinger F, Drenkow J, Zaleski C, Jha S, Batut P, Chaisson M and
711 Gingeras TR. STAR: ultrafast universal RNA-seq aligner. *Bioinformatics*. 2013;29:15-21.
712 70. Wolock SL, Lopez R and Klein AM. Scrublet: Computational Identification of Cell Doublets
713 in Single-Cell Transcriptomic Data. *Cell Syst*. 2019;8:281-291 e9.
714 71. Satija R, Farrell JA, Gennert D, Schier AF and Regev A. Spatial reconstruction of single-
715 cell gene expression data. *Nat Biotechnol*. 2015;33:495-502.
716 72. Wolf FA, Angerer P and Theis FJ. SCANPY: large-scale single-cell gene expression data
717 analysis. *Genome Biol*. 2018;19:15.
718 73. Wang L, Feng Z, Wang X, Wang X and Zhang X. DEGseq: an R package for identifying
719 differentially expressed genes from RNA-seq data. *Bioinformatics*. 2010;26:136-8.
720 74. Schmittgen TD and Livak KJ. Analyzing real-time PCR data by the comparative C(T)
721 method. *Nature protocols*. 2008;3:1101-8.
722
723

Acknowledgments

We thank Dr. Dennis Lewandowski in the Heart Center at the Nationwide Children's Hospital for his critical reading and editing of the manuscript.

Author contributions

J.J. and D.L. conceived and designed the study, analyzed the experiments, wrote the paper. M.B and M.L performed scRNA-Seq data analysis. Y.J.K and E.K. performed the experiments. C.C. provided *Tnnt2*$^{nGFP/+}$ mice. V.G., J.J. and D.L. edited manuscript. All authors reviewed the results and approved the final version of the manuscript.

Competing Interests

None.

Sources of Funding

This work was partially supported by the National Heart, Lung, and Blood Institute R01 grant HL153406 (D. L.), American Heart Association (AHA)-Career Development Award 23CDA1046244 and AHA-Innovative Project Award 23IPA1048560 (J. J.).

742 **Figures and Figure legends**

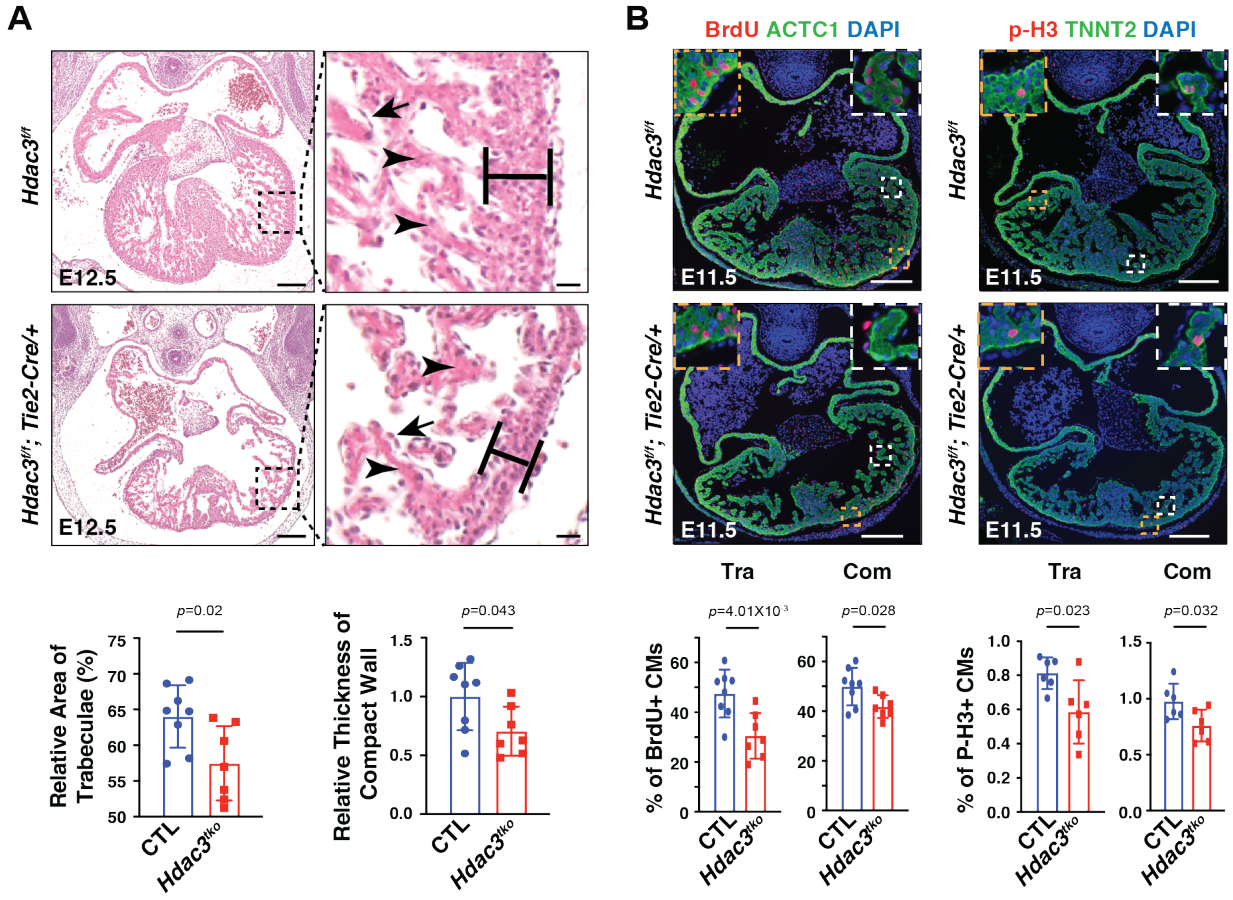

743

744 **Figure 1. Endothelial specific deletion of *Hdac3* results in hypotrabeculation.**

745 **(A)** Hematoxylin and eosin staining on cross sections of an E12.5 *Hdac3*^{tko} embryo
746 (*Hdac3*$^{f/f}$*; Tie2-Cre/+*) and a littermate control (CTL) embryo (*Hdac3*$^{f/f}$). Arrows mark
747 endocardium and arrowheads point to trabeculae. Quantifications are shown on the
748 bottom (CTL: n=8, *Hdac3*^{tko}: n=7). Scale bars, 200 μm (main panels) and 25 μm (insets).
749 **(B)** Decreased cardiomyocyte (CM) proliferation in E11.5 *Hdac3*^{tko} hearts.
750 Immunofluorescence staining of Bromodeoxyuridine/5-bromo-2'-deoxyuridine (BrdU) and
751 phospho-Histone H3 (p-H3) staining. High-power Images in the trabecular myocardium
752 (Tra) and in the compact myocardium (Com) are highlighted in white and yellow boxes
753 respectively. Scale bars, 200 μm. Quantification of proliferation index in the trabecular

754 and compact myocardium respectively are shown on the bottom. BrdU (CTL: n=8,
755 *Hdac3*^{tko}: n=7); p-H3 (n=6 in each group). *P*-values were determined by unpaired two
756 tailed Student's *t*-test.

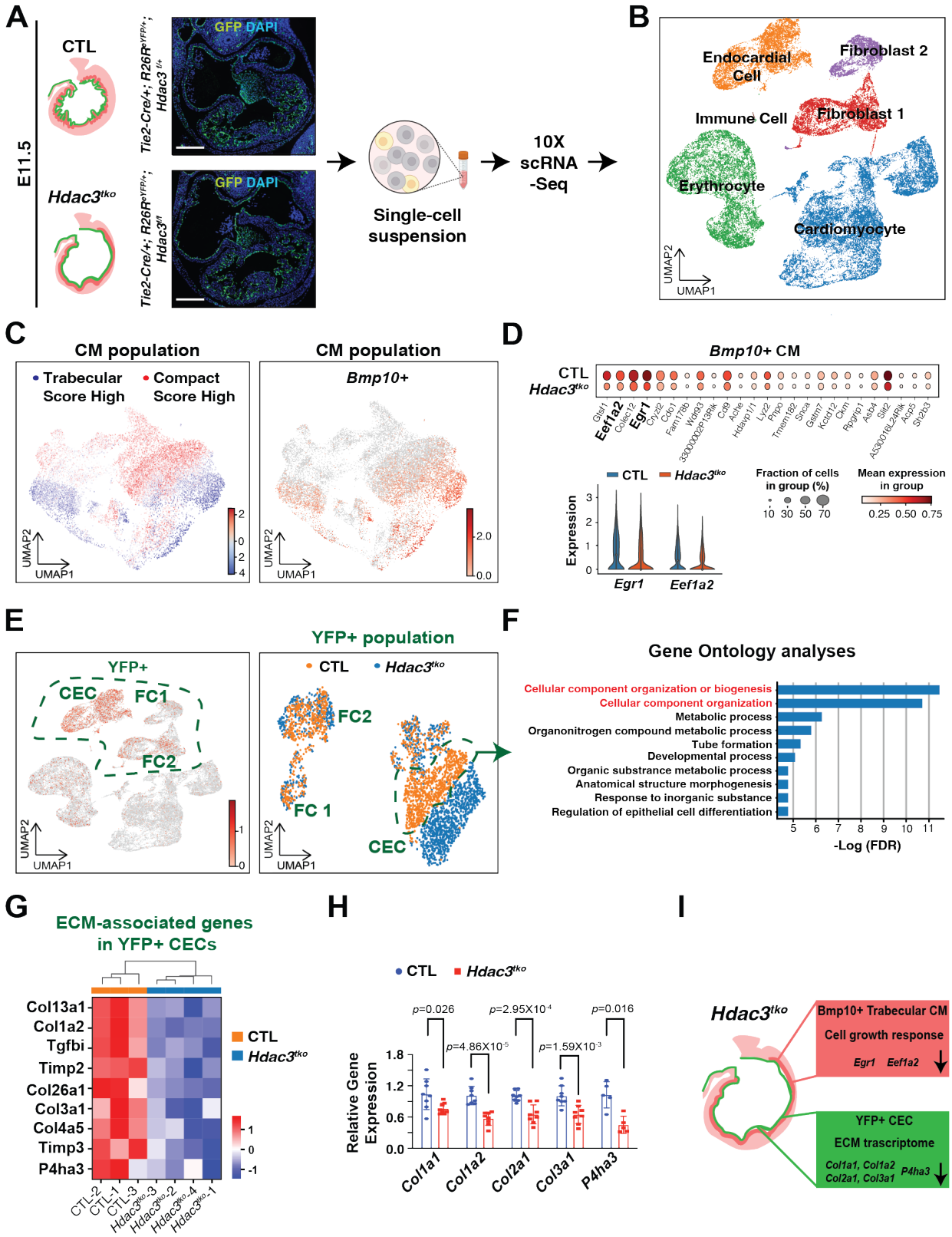
A
CTL
E11.5
Hdac3tko
GFP DAPI
Single-cell suspension
10X scRNA -Seq
B
Endocardial Cell
Fibroblast 2
Immune Cell
Fibroblast 1
Erythrocyte
Cardiomyocyte
UMAP2
UMAP1
C
CM population
Trabecular Score High
Compact Score High
Bmp10+
D
Bmp10+ CM
CTL
Hdac3tko
Fraction of cells in group (%)
Mean expression in group
Expression
Egr1
Eef1a2
E
YFP+
CEC
FC1
FC2
YFP+ population
F
Gene Ontology analyses
Cellular component organization or biogenesis
Cellular component organization
Metabolic process
Organonitrogen compound metabolic process
Tube formation
Developmental process
Organic substrance metabolic process
Anatomical structure morphogenesis
Response to inorganic substance
Regulation of epithelial cell differentiation
-Log (FDR)
G
ECM-associated genes in YFP+ CECs
Col13a1
Col1a2
Tgfbi
Timp2
Col26a1
Col3a1
Col4a5
Timp3
P4ha3
H
Relative Gene Expression
p=0.026
p=4.86X10-5
p=2.95X10-4
p=1.59X10-3
p=0.016
Col1a1
Col1a2
Col2a1
Col3a1
P4ha3
I
Bmp10+ Trabecular CM
Cell growth response
YFP+ CEC
ECM trascriptome

758 **Figure 2. Single-cell RNA sequencing reveals decreased expression of ECM genes**
759 **in *Hdac3^{tko}* hearts.**
760 **(A)** Schematic workflow of scRNA-Seq experimental design. Representative micrographs
761 of GFP immunofluorescence staining of E11.5 *Hdac3^{tko}* embryo (*Hdac3$^{f/f}$; Tie2-Cre/+;*
762 *R26R$^{eYFP/+}$*) and a littermate control (CTL) embryo (*Hdac3$^{f/+}$; Tie2-Cre/+; R26R$^{eYFP/+}$*).
763 Scale bars, 250 μm. **(B)** UMAP visualization of cell populations in an E11.5 control heart.
764 **(C)** Trabecular and compact cardiomyocyte (CM) score were calculated within *Tnni*+ CM
765 population. Left UMAP showed CMs split into a lower cluster that has a high trabecular
766 score, and an upper cluster that has a high compact score. Right UMAP shows the
767 expression level of *Bmp10*+ per cell. **(D)** Dot plots of differentially expressed genes in
768 *Hdac3^{tko}* and CTL trabecular clusters. Violin plots of expression of *Egr1* and *Eef1a2* in
769 *Hdac3^{tko}* and CTL trabecular clusters. **(E)** The UMAP on the left shows that YFP+ cells
770 are distributed in cardiac endothelial cell (CEC, *Cdh*+), fibroblast cell 1 (FC1, *Pdgfra*+),
771 and fibroblast cell 2 (FC2, *Dcn*+) clusters. The overlapping UMAPs of *Hdac3^{tko}* and CTL
772 YFP+ cells are shown on the right. **(F)** Gene Ontology pathway analysis of top marker
773 genes in CTL-specific YFP+ CEC cluster (Cut off value: -log (FDR)>5). **(G)** Heatmap of
774 extracellular matrix (ECM) associated genes in E11.5 *Hdac3^{tko}* and CTL hearts. Data
775 were extracted from YFP+ CEC clusters in the scRNA-Seq dataset. **(H)** qRT-PCR
776 analysis of *Col1a1*, *Col1a2*, *Col2a1*, *Col3a1* and *P4ha3* in E11.5 *Hdac3^{tko}* heart as
777 compared to CTL hearts (n=8 in each group for *Col1a1*, *Col1a2*, *Col2a1* and *Col3a1,* n=5
778 in each group for *P4ha3*). *P*-values were determined by unpaired two tailed Student's *t*-
779 test. (**I)** Illustration of decreased expression of proliferation related genes in trabecular
780 CMs and ECM-associated genes in CECs of *Hdac3^{tko}* hearts.

781

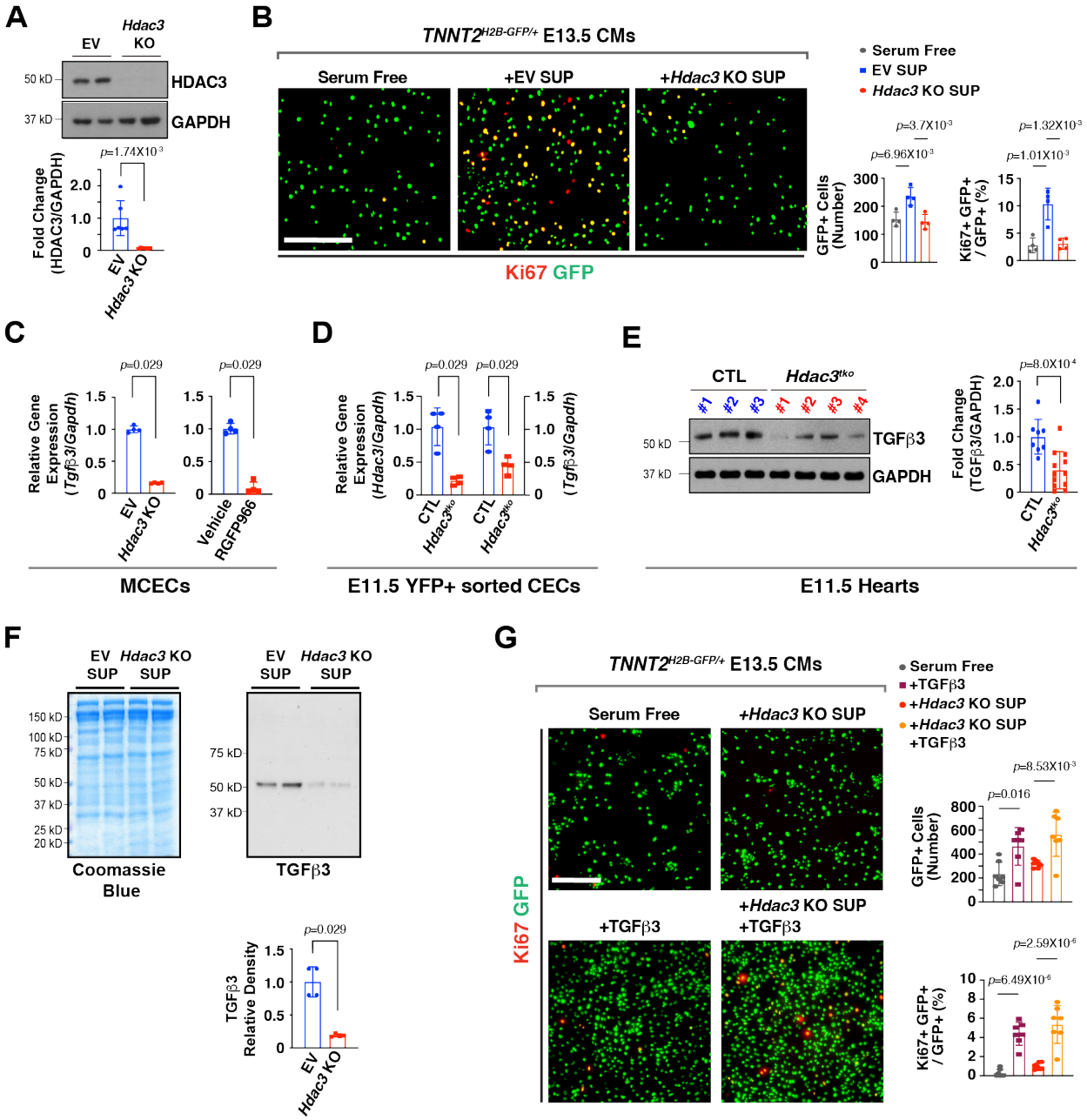
A
Hdac3
EV
KO
50 kD
HDAC3
37 kD
GAPDH
Fold Change (HDAC3/GAPDH)
p=1.74X10-3
EV
Hdac3 KO
B
TNNT2H2B-GFP/+ E13.5 CMs
Serum Free
+EV SUP
+Hdac3 KO SUP
Ki67 GFP
Serum Free
EV SUP
Hdac3 KO SUP
p=3.7X10-3
p=6.96X10-3
p=1.32X10-3
p=1.01X10-3
GFP+ Cells (Number)
Ki67+ GFP+ / GFP+ (%)
C
p=0.029
p=0.029
Relative Gene Expression (Tgfβ3/Gapdh)
EV
Hdac3 KO
Vehicle
RGFP966
MCECs
D
p=0.029
p=0.029
Relative Gene Expression (Hdac3/Gapdh)
(Tgfβ3/Gapdh)
CTL
Hdac3tko
CTL
Hdac3tko
E11.5 YFP+ sorted CECs
E
CTL
Hdac3tko
#1
#2
#3
#1
#2
#3
#4
50 kD
TGFβ3
37 kD
GAPDH
p=8.0X10-4
Fold Change (TGFβ3/GAPDH)
CTL
Hdac3tko
E11.5 Hearts
F
EV SUP
Hdac3 KO SUP
150 kD
100 kD
75 kD
50 kD
37 kD
25 kD
20 kD
Coomassie Blue
EV SUP
Hdac3 KO SUP
75 kD
50 kD
37 kD
TGFβ3
p=0.029
TGFβ3 Relative Density
EV
Hdac3 KO
G
TNNT2H2B-GFP/+ E13.5 CMs
Serum Free
+Hdac3 KO SUP
+TGFβ3
+Hdac3 KO SUP +TGFβ3
Ki67 GFP
Serum Free
+TGFβ3
+Hdac3 KO SUP
+Hdac3 KO SUP +TGFβ3
p=8.53X10-3
p=0.016
GFP+ Cells (Number)
p=2.59X10-6
p=6.49X10-6
Ki67+ GFP+ / GFP+ (%)

782 **Figure 3. Cardiac endothelial *Hdac3* knockout results in downregulation of TGFβ3**
783 **and decreased cardiomyocyte proliferation.**
784 **(A)** Generation of *Hdac3* knockout (KO) and empty vector control (EV) mouse cardiac
785 endothelial cells (MCECs) by CRISPR/Cas9. Deletion of *Hdac3* was verified by western
786 blot. Quantification is shown below (n=6 in each group). **(B)** The effects of *Hdac3* KO
787 MCEC supernatants on E13.5 *Tnnt2*$^{nGFP/+}$ cardiomyocytes (CM) proliferation.
788 Representative immunofluorescence micrographs are shown. Scale bar, 275 μm.
789 Percentage of Ki67+ CMs and total number of GFP+ CMs were quantitated (n=4 in each
790 group). **(C)** Quantification of *Tgfβ3* expression in *Hdac3* KO MCECs, or RGFP966-treated
791 MCECs (10 uM) by qRT-PCR. *Gapdh* was used as cDNA loading control (n=4 in each
792 group). **(D)** Downregulation of *Tgfβ3* gene expression in *Hdac3* deficient cardiac
793 endothelial cells. YFP+ E11.5 cardiac endothelial cells (CECs) from *Hdac3*^{tko} (*Hdac3*$^{f/f}$*;*
794 *Tie2-Cre/+; R26*$^{eYFP/+}$) and CTL (*Hdac3*$^{f/+}$*; Tie2-Cre/+; R26*$^{eYFP/+}$) hearts were sorted by
795 fluorescence-activated cell sorting. Quantification of *Hdac3* and *Tgfβ3* expression by
796 qPCR was shown on the right. n=4 for each group. *Gapdh* was used as cDNA loading
797 control (n=4 in each group). **(E)** Representative Western blot and quantification of TGFβ3
798 expression in E11.5 *Hdac3*^{tko} hearts (n=12) and littermate CTL hearts (n=8). **(F)** Secretion
799 of TGFβ3 from *Hdac3* KO and EV MCECs. Coomassie brilliant blue staining of total
800 extracted proteins from supernatants served as protein loading controls. TGFβ3 in the
801 MCEC supernatants were detected by western blot. Quantifications are shown on the
802 right (n=4 in each group). **(G)** Rescue of CM proliferation defect by *Hdac3* KO MCECs
803 supernatant supplemented with recombinant TGFβ3 (working concentration: 250 ng/ml).
804 Representative immunofluorescence micrographs are shown. Scale bar, 200 μm.

805 Percentage of Ki67+ CMs and total number of GFP+ CMs were quantitated (n=7 in each
806 group). *P*-values were determined by unpaired two tailed Student's *t*-test for **(A)** and **(E)**,
807 Mann-Whitney U test for **(C)**, **(D)** and **(F)** and one-way ANOVA followed by the Tukey
808 post hoc test for **(B) and (G)**.
809

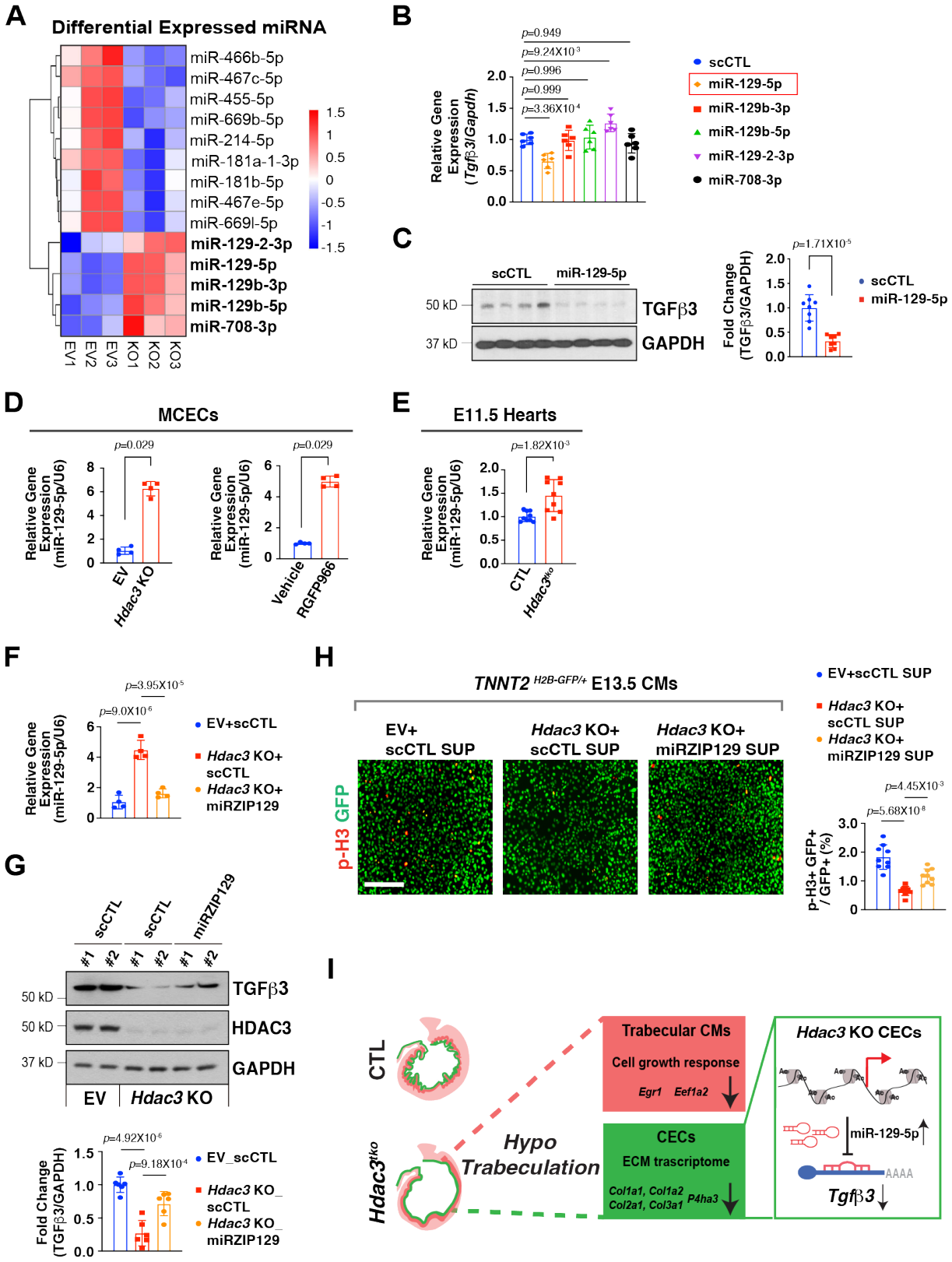
A
Differential Expressed miRNA
miR-466b-5p
miR-467c-5p
miR-455-5p
miR-669b-5p
miR-214-5p
miR-181a-1-3p
miR-181b-5p
miR-467e-5p
miR-669l-5p
miR-129-2-3p
miR-129-5p
miR-129b-3p
miR-129b-5p
miR-708-3p
EV1 EV2 EV3 KO1 KO2 KO3
B
Relative Gene Expression (Tgfβ3/Gapdh)
p=0.949
p=9.24X10-3
p=0.996
p=0.999
p=3.36X10-4
scCTL
miR-129-5p
miR-129b-3p
miR-129b-5p
miR-129-2-3p
miR-708-3p
C
scCTL
miR-129-5p
50 kD
37 kD
TGFβ3
GAPDH
Fold Change (TGFβ3/GAPDH)
p=1.71X10-5
D
MCECs
Relative Gene Expression (miR-129-5p/U6)
p=0.029
EV
Hdac3 KO
Vehicle
RGFP966
E
E11.5 Hearts
p=1.82X10-3
CTL
Hdac3tko
F
p=3.95X10-5
p=9.0X10-6
EV+scCTL
Hdac3 KO+ scCTL
Hdac3 KO+ miRZIP129
G
scCTL
miRZIP129
#1 #2
TGFβ3
HDAC3
GAPDH
EV
Hdac3 KO
p=4.92X10-6
p=9.18X10-4
EV_scCTL
Hdac3 KO_ scCTL
Hdac3 KO_ miRZIP129
H
TNNT2 H2B-GFP/+ E13.5 CMs
EV+ scCTL SUP
Hdac3 KO+ scCTL SUP
Hdac3 KO+ miRZIP129 SUP
p-H3 GFP
p=4.45X10-3
p=5.68X10-8
p-H3+ GFP+ / GFP+ (%)
I
CTL
Hdac3tko
Hypo Trabeculation
Trabecular CMs
Cell growth response
Egr1 Eef1a2
CECs
ECM trascriptome
Col1a1, Col1a2 Col2a1, Col3a1 P4ha3
Hdac3 KO CECs
miR-129-5p
AAAA
Tgfβ3

810

811 **Figure 4. HDAC3 induces Tgfβ3 by repressing miR-129-5p.**

812 **(A)** Heatmap of microRNA (miR) sequencing of *Hdac3* knockout (KO) and empty vector
813 control (EV) mouse cardiac endothelial cells (MCECs). MiRs with reads less than 100
814 were discarded and miRNA expression levels were normalized by TPM (transcript per
815 million) values (TPM = [miRNA total reads/total clean reads] × 10^6). Log_2 fold changes
816 were calculated by TPM per miR in the KO group divided by the mean TPM per miR in
817 the EV group then followed by calculation of Log (fold change, 2). Significantly
818 downregulated miRs are shown in blue, and significantly up-regulated miRs are shown in
819 red. Cut-off criteria: Log2>1.5 and adjusted *P*-value<0.01. **(B)** Quantification of the
820 expression of *Tgfβ3* in MCECs after miR mimics treatment (final concentration 10 nM) by
821 qRT-PCR. *Gapdh* was used as a cDNA loading control (n=6 in each group). Relative
822 gene expression was compared to the miR scrambles (scCTL) group. **(C)** Representative
823 Western blot and quantification of the expression of TGFβ3 after miR-129-5p mimics
824 treatment by western blot (n=8 in each group). **(D)** (Left) Quantification of *Tgfβ3*
825 expression in *Hdac3* KO and EV MCECs (n=4 in each group). (Right) Quantification of
826 the expression of *Tgfβ3* in MCECs after Hdac3 inhibitor treatment (RGFP966, final
827 concentration 5 uM) (n=4 in each group). **(E)** Quantification of the expression of *Tgfβ3* in
828 *Hdac3^{tko}* heart lysates (n=9 in each group). **(F)** Quantification of the expression of miR-
829 129-5p by qRT-PCR**.** *Hdac3* KO or EV MECs were transfected with LentimiRa-GFP-
830 miRZip129 (miRZIP129) or pGreenPuro Scramble Hairpin control lentivirus (scCTL) and
831 transfected cells were selected using puromycin (n=4 in each group)**. (G)** Representative
832 Western blot and quantification of the expression of TGFβ3 after treatment with
833 miRZIP129 or scCTL in *Hdac3* KO and EV MCECs (n=6 in each group). **(H)** Knockdown

834 of miR-129-5p rescues CM proliferation deficit induced by *Hdac3* KO MCEC supernatants.
835 Representative immunofluorescence micrographs are shown. Scale bar, 200 μm.
836 Quantification of percentage of phospho-histone H3 (p-H3)+ CMs was shown on the right.
837 Independent samples: n=9 in each group. The protein expression of TGFβ3 *P*-values
838 were determined by unpaired two tailed Student's *t*-test for **(C)** and **(E)**, the Mann-Whitney
839 U test for **(D)** and the one-way ANOVA followed by Tukey post hoc test for **(B)**, **(F)**, **(G)**
840 and **(H)**. **(I)** Working model: in the developing endocardium, HDAC3 represses the
841 expression of miR-129-5p to release their suppression on the expression of TGFβ3.
842 When *Hdac3* is deleted, the expression of miR-129-5p is increased, which subsequently
843 suppresses the expression of TGFβ3 to a stronger extent, and the decrease of TGFβ3,
844 together with decreased ECM, leads to hypotrabeculation.